Available online at www.sciencedirect.com
SCIENCE DIRECT®
Ecological Modelling 186 (2005) 312–325
ECOLOGICAL MODELLING
www.elsevier.com/locate/ecolmodel

Quantifying spatial structure of volumetric neutral models

Lee Anne Kirkpatrick [a], John F. Weishampel [b,*]

[a] *Liberal Studies Program, University of Central Florida, Orlando, FL 32816-2368, USA*
[b] *Department of Biology, University of Central Florida, 4000 Central Florida Blvd, Orlando, FL 32816-2368, USA*

Received 11 June 2004; received in revised form 31 December 2004; accepted 7 January 2005
Available online 26 February 2005

Abstract

Neutral models in landscape ecology that have been used as a framework to analyze actual landscapes have been largely planar. However, the natural world is greater than two dimensions; hence, many ecological structures, e.g., forest canopies or coral reefs, are better represented by topographies or tomographies. Because pattern and process or structure and function are intertwined, it becomes necessary to develop methods to quantify these complex architectures. With the advent of remote sensing technologies such as lidars and sonars, that permit structural mapping of some of these systems, volumetric data are becoming more prevalent. In this study, we developed a suite of binary voxel-based neutral models that possessed random, anisotropic, and hierarchical properties. We then evaluated the extent to which fractal-derived measurements, i.e., lacunarity, the simple fractal dimension, and multifractal spectra, were able to discern among the constructed model types at two different densities ($p = 0.02$ and $p = 0.05$). Multifractal analysis, where spectra were defined by three parameters, was shown to be the most sensitive to the differences among the neutral structures. Lacunarity, defined by a single parameter, was shown to be fairly useful in discerning the structures. The simple fractal dimension was found to have limited capability. To more fully assess the ability of these and additional pattern recognition methods, better representations of natural morphologies need to be developed and analyzed.

Keywords: Forest canopy; Lacunarity; Multifractal; Neutral landscape model; Three-dimensional architecture; Voxel

"Distress not yourself if you cannot at first understand the deeper mysteries of Spaceland."

—A. Square a.k.a. E.A. Abbott (1884) in *Flatland: A Romance of Many Dimensions*

1. Introduction

The role of neutral models, like that of the null hypothesis, has been to provide a standard by which to compare observations (Caswell, 1976; Taylor, 1979; Thomas and Foin, 1982; Gotelli and Graves, 1996). In the field of landscape ecology, the neutral landscape model (NLM), void of all biotic and abiotic factors thought to contribute to the landscape structure, de-

* Corresponding author. Tel.: +1 407 823 6623; fax: +1 407 823 5769.
E-mail address: jweisham@mail.ucf.edu (J.F. Weishampel).

0304-3800/$ – see front matter © 2005 Elsevier B.V. All rights reserved.
doi:10.1016/j.ecolmodel.2005.01.056

fines an assumed or predicted pattern that functions as a baseline for studying real landscape data (Gardner et al., 1987; Turner et al., 1989; Milne, 1992; With and Crist, 1995; With and king, 1997; Hargrove et al., 2002). Thus far, neutral models in landscape ecology have mostly consisted of randomly or systematically generated fractal planes, i.e., structures between one and two dimensions (Gardner et al., 1987; O'Neill et al., 1988; Turner et al., 1989; Gardner and O'Neill, 1991). These grid-based maps often derived from percolation theory (Stauffer, 1985; Gardner et al., 1987) are compatible for comparison to landscape data found on raster maps generated by geographical information systems (GIS) (With et al., 1997). Neutral to the ecological processes that affect the patterns of real landscapes, two-dimensional NLMs simulate fully random distributions of habitat (e.g., Gardner et al., 1987; Wiens et al., 1997) or by using more sophisticated algorithms, mimic more spatially explicit structural patterns such as those found in gradient (Keitt and Johnson, 1995; Milne et al., 1996), hierarchical (O'Neill et al., 1992; Lavorel et al., 1993; Gardner et al., 1993; Pearson et al., 1996) and fractal (Palmer, 1992; Moloney and Levin, 1996; With et al., 1997) landscapes.

However, many landscape structures, as well as other natural systems in and out of the field of ecology, are better represented by fractal surfaces or volumes, i.e., structures between two and three dimensions. Coral reefs (Basillais, 1998), soil pedons (Rappoldt and Crawford, 1999), plankton distributions (Gallager et al., 1996), root system architecture (Fitter and Strickland, 1992), fracture networks in rock (PyrakNolte et al., 1997), and the microarchitecture of bone (Dougherty and Henebry, 2002) are a few examples of such volumetric structures that can be depicted as fractal sponges with occupied and empty spaces (Moffett, 2001). Additionally, simulations of the geometry of insect movements influenced by plant canopy architecture (Casas and Aluja, 1997; Skirvin, 2004), bacterial aggregation (Dechesne et al., 2003), earthworm burrows (Capowiez et al., 2001), and grouping behaviors such as bees swarming or fish schooling (Parrish and Hamner, 1997) require a three-dimensional framework.

To fully address questions of how structure relates to function, it is necessary to accurately quantify the structure of a system. For instance, forest canopy architecture has been deemed the key to forest ecosystem processes (Spies, 1998) and the master regulator of the forest (Hallé et al., 1978). The volumetric distribution of leaves, branches, twigs, etc. influences the canopy environment, tree physiology, atmospheric exchange, and biotic habitat (Nadkarni et al., 1996). Though tropical rain forest canopies are considered to be the most biodiverse and architecturally complex ecosystems, we do not understand how or to what extent species richness relates to structure. Thus, we do not know how disturbances, such as selective logging, which alter canopy structure in turn affect species diversity. However, along these lines, spatially explicit forest models have been used to simulate disturbances to create volumetric patterns of light availability (Chave, 1999; Dubé et al., 2005) to address structure–function relationships.

Volumetric mapping of some of these three-dimensional systems has become available by way of recent technology. Positron emission tomography (PET), ultrasonography (US), real-time three-dimensional ultrasound (RT3D), and magnetic resonance imaging (MRI) produce volumetric images allowing for measurements and comparative study in diagnostic medicine (Sisodiya et al., 1996; Downey et al., 2000; Stetten and Tamburo, 2001; Aykac et al., 2002). X-ray computerized tomographic (CT) imaging is used for quantifying three-dimensional interconnected fracture networks in opaque rock samples (PyrakNolte et al., 1997). Improved acoustic sampling techniques used in fishery research are used to estimate the volumetric density and spatial structure of animal distributions over a range of scales (Hewitt and Demer, 2000). In studies of forested systems, lidar remote sensing acquires data enabling the rendering of volumetric canopy structure (see Fig. 1; Weishampel et al., 2000; Lefsky et al., 2002). This revolutionary ability to envision the distribution of canopy components (i.e., leaves, branches, trunks, epiphytes, etc.) in three-dimensional space (Turner et al., 2003; Gillespie et al., 2004; Parker et al., 2004) requires volumetric versions of the neutral landscape model for comparison.

As landscape ecology focuses on the causes and consequences of spatial heterogeneity across a range of scales (Turner et al., 2001), numerous pattern analysis techniques and indices have been developed for quantifying spatial variations of ecosystems using planar maps (Li and Reynolds, 1994; Gustafson, 1998). How these methods respond to variations in

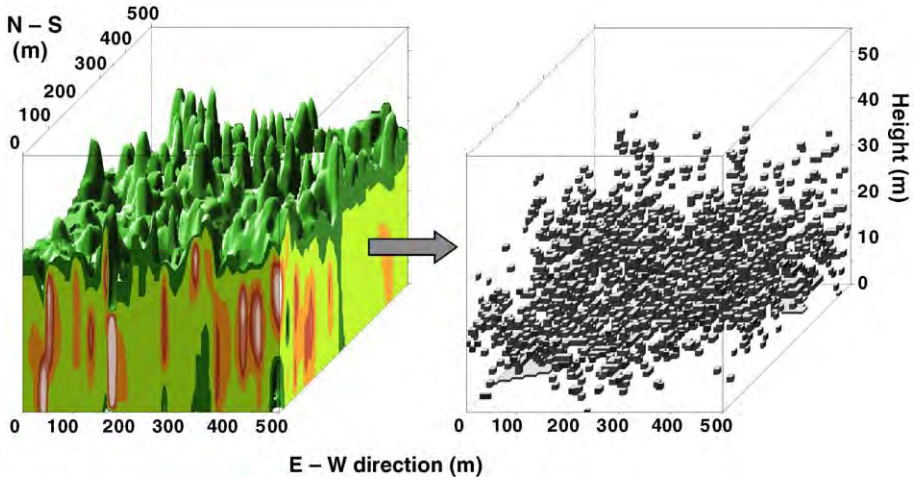

Fig. 1. Volumetric rendering of 25 ha of primary rainforest from Barro Colorado Island, Panama based on returns (left) from the Lidar Vegetation Imaging Sensor (see Weishampel et al., 2000). Yellow-brown-beige regions represent areas with higher returns that correspond to higher densities of reflecting components. The corresponding upper 2% of ~1 m vertical returns within each ~10 × 10 m interpolated area is shown by the binary transformation (right). The vertical axis is exaggerated. (For interpretation of the references to colour in this figure legend, the reader is referred to the web version of the article.)

spatial heterogeneity of volumetric structures has not been explored. To address this issue, we developed binary cubic counterparts (minimum unit = voxel) to the flat crossword puzzle-like (minimum unit = pixel) neutral models based on percolation and fractal theory. Three pattern analysis techniques based on fractal (Mandelbrot, 1983) measures were selected for their ready adaptability to three-dimensional pattern analysis. Here, we report the extent to which these techniques were able to discern differences among the volumetric neutral models.

2. Methods

Neutral percolation models were constructed on a 50 × 50 × 50 cubic lattice framework. These dimensions roughly correspond to those used to bin lidar returns in forest canopy studies (Weishampel et al., 2000; Parker et al., 2004). Models were built with $p = 0.02$ (low) and $p = 0.05$ (high) overall concentrations of occupied cells. The six model types consisted of occupied and unoccupied cubic spaces (Fig. 2) that were spatially random or organized following gradient or hierarchical rules. Each of the model types for high and low density conditions was replicated 10 times. Three pattern analysis techniques, lacunarity (see Dale, 2000), simple fractal (see Sugihara and May, 1990), and multifractal spectra (see Scheuring and Riedi, 1994), were used to quantify the 120 binary structures. For each density, an ANOVA approach was used to assess the capability of each technique to detect pattern differences among the models in a manner comparable to Li and Reynolds (1994).

2.1. Construction of neutral models

Algorithms for each binary volumetric model type (Fig. 2) were written according to the following percolation rules:

(a) Fully random (RND): Each cell was randomly designated as occupied or unoccupied.
(b) Gradient (GRD): The cells within each layer of the lattice were randomly occupied with linearly increasing probability, the bottom layer having the lowest probability of occupancy and the top layer, the highest (sparse: from $p = 0$ to 0.03; dense: from $p = 0$ to 0.09).
(c) Split gradient (SGD): Similar to the gradient rules, the lower half of the structure was generated with a linearly increasing probability of occupation (sparse: from $p = 0.002$ to 0.04; dense: from $p = 0.004$ to 0.10), the upper half with linearly de-

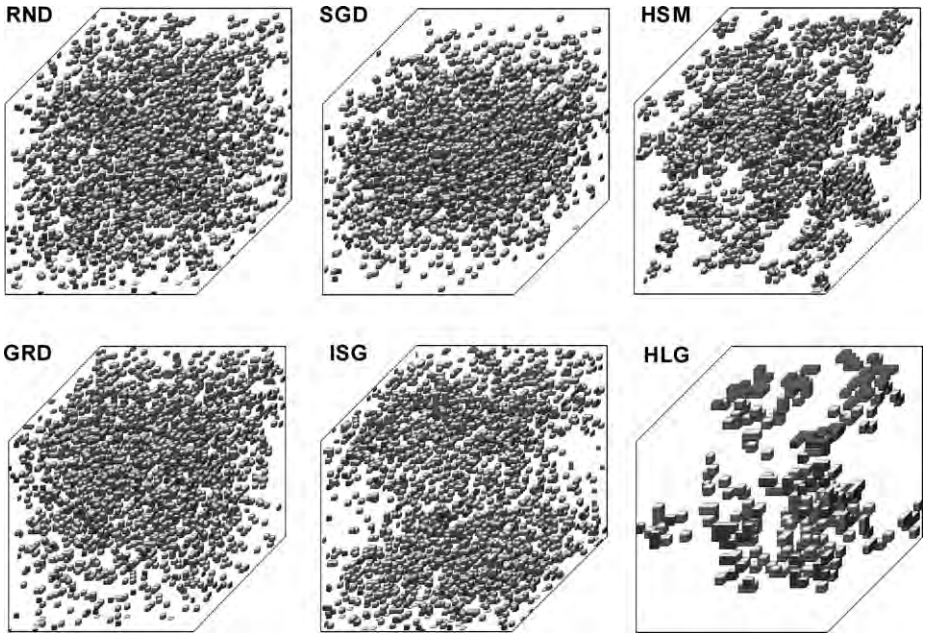

Fig. 2. Examples of the volumetric neutral models with $p = 0.02$.

creasing probability (sparse: from $p = 0.04$ to 0.002; dense: from $p = 0.10$ to 0.004). Thus, the occupied voxels were concentrated in the middle of the volume.

(d) Inverse split gradient (ISG): The upper half of the volume was generated with a linearly decreasing proportion of occupied cells (sparse: from $p = 0.04$ to 0.002; dense: from $p = 0.10$ to 0.004), which was mirrored by the lower half. Thus, the occupied voxels were concentrated at two opposite faces of the volume.

(e) Hierarchical small (HSM): Curdling methods (Mandelbrot, 1983; Lavorel et al., 1993) were used to simulate a two-level (broad and fine scale) fragmented hierarchical landscape with small gaps and clusters. At the first level (broad scale), $5 \times 5 \times 5$ cubic clusters were randomly removed from a fully occupied cubic matrix with $p_1 = 0.2$ for sparse models and $p_1 = 0.5$ for dense models. At the second level (fine scale), $1 \times 1 \times 1$ unit cells were removed from the remaining occupied sites with $p_2 = 0.1$ for both sparse and dense models.

(f) Hierarchical large (HLG): In a fashion similar to the HSM methods, $10 \times 10 \times 10$ blocks were removed followed by the removal of $2 \times 2 \times 2$ blocks to mimic a hierarchical landscape with large gaps and clusters. The same probabilities used to generate HSM models determined the number of occupied sites at each level of the HLG models.

2.2. Structural analysis techniques

2.2.1. Lacunarity

The first technique tested for its ability to discern volumetric patterns was lacunarity, a measure of pattern texture. Lacunarity (Λ), the word derived from "lacuna" meaning "gap" or "missing section," in this context refers to the distribution of gap sizes within the binary structures. Gefen et al. (1983) defined lacunarity as a measure of the deviation of an object from translational invariance or homogeneity. Objects with a wide range of gap sizes (heterogeneous) have higher lacunarity measures than objects with similar sized gaps (homogeneous). However, the same object may be heterogeneous at small scales (high lacunarity) but be homogeneous at broad scales (low lacunarity) (Gefen et al., 1983).

In addition to being scale-dependent, Plotnick et al. (1993) point out that lacunarity is also a function of density and pattern. Maps with similar geometric

shapes, for example a fully random map, with fewer occupied sites will tend to be gappier than denser maps and, thus, will have higher lacunarity. If occupied sites tend to clump together in one map, but in contrast are randomly situated in another map of equal density, the former will tend to have higher lacunarity than the latter. The more regular the pattern, the less variance there will be between box masses. In a perfect checkerboard pattern, for instance, no variance will exist. In such a case, $\Lambda = 1$ (Plotnick et al., 1993).

To find the lacunarity measures of the volumetric models, a three-dimensional version of the 'gliding box' algorithm developed by Allan and Cloitre (1991) was applied to each model. The lacunarity, $\Lambda(r_{xyz})$, was calculated at a range of scales. Beginning at (1, 1, 1), a box of size $r_{xyz} = 1$ was placed over the first voxel. If the site was occupied, its box mass, S, was 1. The box was advanced one unit at a time through the cubic lattice and each box mass was calculated. The procedure was repeated for $r_{xyz} = 2$ through 25, counting the box mass, or number of occupied sites, within each box size. From the first and second statistical moments, $Z^{(1)}$ and $Z^{(2)}$, of the probability distribution, $Q(S,r_{xyz})$, the lacunarity was calculated as

$$\Lambda(r_{xyz}) = \frac{Z^{(2)}}{(Z^{(1)})^2} \tag{1}$$

where

$$Z^{(1)} = \sum_{S=0}^{r_{xyz}^2} SQ(S, r_{xyz}) \tag{2}$$

and

$$Z^{(2)} = \sum_{S=0}^{r_{xyz}^2} S^2 Q(S, r_{xyz}) \tag{3}$$

(Gefen et al., 1983; Plotnick et al., 1993, 1996; Cheng, 1997a,b; Dale, 2000; Weishampel et al., 1998, 2001). Each curve from the log–log plots of lacunarity versus box size for each replicate were fit to an exponential decay function,

$$\Lambda(r_{xyz}) = a\mathrm{e}^{-br} \tag{4}$$

where a and b are constants. The value of a represents $\Lambda(1)$, and is a function of the probability of occupancy $\Lambda(1) = 1/\mathrm{p}$. Consequently, for $p = 0.02$, $\Lambda(1) = 50$ and for $p = 0.05$, $\Lambda(1) = 20$. The constant b characterizes the rate of decay and the shape of the best-fit curve and is, thus, the parameter used for comparing the lacunarity of the structural patterns.

2.2.2. Simple fractal dimension

The second measure studied for its capability in discerning volumetric patterns was the fractal or fractional dimension, D_f. The fractal dimension is "a way to measure how rough fractal curves [or surfaces] are" (Green, 1995). Another definition for fractal dimension to which Green (1995) alluded is how well a curve or surface fills space. For example, a very rough curve (e.g., a rocky coastline) with many jagged corners might come close to filling a surface, in which case the curve would come closer to having a dimension of 2 rather than 1. Similarly, a rough surface (e.g., a rugged mountain range) would have somewhere between two and three dimensions. Fractal dimensions can be any real number within the intervals [0,1], [1,2] or [2,3] and, like lacunarity measures, are scale-dependent, capturing changes in a pattern over many resolutions.

The fractal dimensions of the 120 neutral structures were calculated by using a voxel-counting algorithm for three-dimensional space following:

$$D_\mathrm{f} = -\lim_{\varepsilon_{xyz}\to 0}\left(\frac{\log N(\varepsilon_{xyz})}{\log \varepsilon_{xyz}}\right) \tag{5}$$

where $N(\varepsilon_{xyz})$ is the total number of boxes containing at least one occupied cell at each box size whose length (ε_{xyz}) equaled 1 through 25. A regression line was fit to the log–log plot of $N(\varepsilon_{xyz})$ versus ε_{xyz} for each model replicate. The slopes were calculated to find D_f, the second parameter to be assessed for its capability of detecting differences in the volumetric patterns (Mandelbrot, 1983; Sugihara and May, 1990; Zeide, 1991; Mladenoff et al., 1993; Wiens et al., 1995; Bérubé and Jébrak, 1999; Kostylev and Erlandsson, 2001).

2.2.3. Multifractal spectra

Lastly, spectra generated from multifractal analyses were examined for their sensitivity to volumetric pattern variation. Though the fractal dimension exponent can better characterize a fractal object than an integer dimension, the box-counting algorithm described earlier gives equal weight to a box that proportionately

contains less of the object than another box. In other words, the varying mass measures of the subsets are not taken into account in the calculation of the fractal dimension, and thus information is lost. When studying the patterns of structures or systems in nature that are inextricably tied to the underlying processes that create them, the unknown details may be important to the understanding of causal factors (Mandelbrot, 1983; Drake and Weishampel, 2000, 2001). Particularly in complex systems, where local conditions can have profound influence on higher level processes, fine-scale observations are critical.

Considering the importance of information over many scales, complex fractal structures are more accurately expressed as "multifractal sets," fractals that require an infinite number of exponents for their description (Stanley, 1991). To characterize spatial patterns of these fractals within fractals, multifractal techniques have been used to find measures over multiple scaling regions such as are found in many natural systems (Scheuring and Riedi, 1994; Cheng and Agterberg, 1995; Solé and Manrubia, 1995; Cheng, 1997a,b; Drake, 1998; Drake and Weishampel, 2000, 2001; Panahi and Cheng, 2004). To quantify the embedded fractals at varying scales and locations, Falconer (1990) suggests including a scaling exponent, q, that can range from $+\infty$ to $-\infty$, which provides observations of embedded pattern from coarse to fine scales much like changing the zoom of a microscope to change the field of view (Appleby, 1996). The box-counting algorithm of Eq. (5) used to calculate the simple fractal dimension is modified in multifractal analysis to incorporate this approach such that

$$D_{\mathrm{f}} = \lim_{\varepsilon \to 0} \left(\frac{1}{q-1} \right) \frac{\log \sum_{i=1}^{N(\varepsilon)} p_i^q(\varepsilon)}{\log(\varepsilon)} \tag{6}$$

where $N(\varepsilon)$ is the number of boxes of size ε needed to cover the area, $p_i(\varepsilon)$ is the box mass of the ith box and, as already discussed, q is the scaling, or filtering, exponent. The single power-law relationship of the simple fractal dimension ($q = 0$) is expanded to include multiple power-law relationships between the local mass measures and the scalar resolutions at each statistical moment q.

To generate multifractal spectra for all 120 volumetric neutral models, an analysis program developed for planar maps by Drake and Weishampel (2000) from the fixed-size, box-counting algorithm of Mach and Mas (1995, 1997) was modified to accommodate distributions in three-dimensional spatial maps. Twenty-seven spatial resolutions (ε) were selected between 1 and 50 and scaling exponents ranged from $-5 \leq q \leq 10$. Regressions were performed on the output values versus the logarithmic value of the box sizes. Slopes of the fitted lines were calculated to produce the desired multifractal indices, $\tau(q)$, $\alpha(q)$ and $f(\alpha)$:

- $\tau(q)$: The slopes are equivalent to the fractal dimensions of the embedded fractal at each mass measure at each successive spatial resolution corresponding to each filtering exponent or q-value. This spectrum of power-law relationships is $\tau(q)$, referred to as the cumulative generating function.
- $\alpha(q)$: $\alpha(q)$, the derivative of $\tau(q)$, shows the divergence of the pattern from exact self-similarity and can be plotted against q to reveal how the multifractal pattern changes over a range of filters.
- $f(\alpha)$: $f(\alpha)$, a Legendre transform of α such that $f(\alpha) = q\alpha - \tau$, is the set of multifractal measures referred to as the multifractal spectrum of the fractal set.

To prepare to test the sensitivity of multifractal analysis to discern volumetric structural patterns, nonlinear regression techniques were employed to find the best quadratic fits for $f(\alpha)$ versus α, the multifractal measures versus the divergence exponents. The fitted parabolas are the multifractal spectra. The maximum points of the concave down parabolas roughly correspond to D_{f}, the simple fractal dimensions (Solé and Manrubia, 1995). The parameters y_0,c_1, and c_2 from the best quadratic fits to

$$y = y_0 + c_1 x + c_2 x^2 \tag{7}$$

were each studied for their ability to distinguish among the three-dimensional patterns.

2.3. Assessment of structural analysis techniques

Using the regression function from SigmaPlot v. 4.0 (SPSS, 1997), best-fit relationships were determined for the output from each technique. Plots representing multiple spatial scales that correspond to each technique are displayed in Fig. 3 Figs. 3,

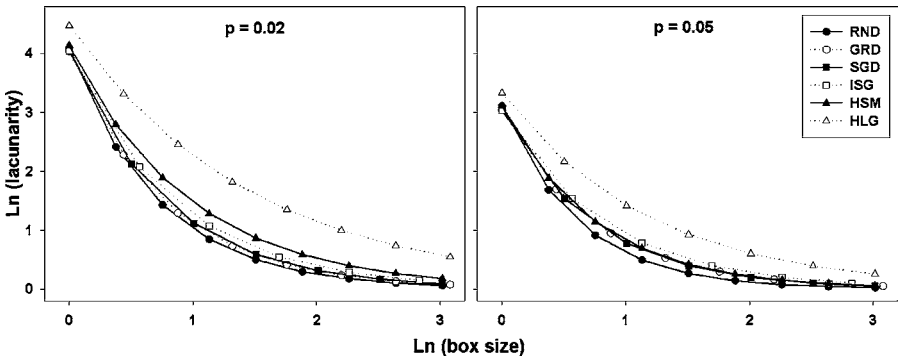

Fig. 3. Exponential decay fits to average lacunarity curves.

5, and 7. To determine whether a pattern analysis technique found significant differences among the different neutral model types for a given occupancy probability, parameter means of b (lacunarity), D_f (mono-fractal), c_1 (multifractal), c_2 (multifractal), and y_0 (multifractal) were compared using an ANOVA approach. Kolmogorov–Smirnov (K–S) tests were performed and normal probability plots (NPP) were evaluated to check for violations of normality. Levene's F-test (L) was used to check for possible heteroscadasticity. Extreme values were checked using Dixon's rankings to detect significant outlier points. A significance level of $\alpha = 0.05$ was the cutoff for all statistical assessments. Post hoc comparisons were done using Tukey–Kramer (T–K) procedures. Nonparametric equivalents to the ANOVA, i.e., Mood Median and Kruskal–Wallis, and Tukey–Kramer, i.e., Mann–Whitney, procedures were used when violations of normality or homogeneity could not be corrected by data transformations. These procedures were also used to validate ANOVA results when assumptions were violated.

3. Results

3.1. Lacunarity

The exponential decay fits on the average lacunarity curves on log–log plots of lacunarity as a function of box size are presented in Fig. 3. R^2 values are shown in Table 1. All curves were nonlinear, indicating that the patterns deviate from self-similarity. If patterns were self-similar fractals, the plots would be linear indicating no change of texture with box size. Deviations from linearity on lacunarity plots also give a clue to the presence of multifractal structure. As expected, lacunarity of the sparse models was higher than the lacunarity of the dense models, indicating more gap variation in the sparse models, especially at finer scales (smaller box sizes).

In both plots, the lacunarity of HLG was much higher than the lacunarity of the other models especially RND, indicating less similarity among different locations within the hierarchical structure. Because the HLG had a wider range of gap sizes, it exhibited

Table 1
Mean R^2 values for best-fit equations to the lacunarity, mono-fractal, and multifractal curves for each model type at each occupancy probability

	Lacunarity		Mono-fractal		Multifractal	
	$p = 0.02$	$p = 0.05$	$p = 0.02$	$p = 0.05$	$p = 0.02$	$p = 0.05$
RND	0.98	0.99	0.91	0.94	1.00	0.99
GRD	0.99	1.00	0.91	0.95	0.99	0.97
SGD	0.99	1.00	0.91	0.95	0.99	0.97
ISG	0.99	0.99	0.91	0.95	0.99	0.96
HSM	0.97	0.99	0.93	0.95	0.98	0.97
HLG	0.89	0.94	0.94	0.95	0.99	0.97

greater aggregation of occupied sites. The sparse gradient models were more homogeneous than the hierarchical models and have only slightly higher lacunarity than RND. Higher lacunarity was found in HSM than for other sparse models. But among the dense models, HSM curves were not distinguishable from GRD and SGD and only slightly distinguishable from ISG. This would suggest that with greater density the distribution of gap sizes becomes more similar among these models. RND had the lowest lacunarity, which was not surprising because the gap distributions were more regular in RND when compared to the other models.

Distributions of the parameter data from both the sparse and dense models are displayed in Fig. 4. Though the formal test results indicated no significant deviation from normality (K–S: $p = 0.18$) for the sparse models, the subjective tests showed conflicting evidence (NPP: sigmoidal shape). The test for constant variance across sparse model types gave a strong indication of heteroscedasticity. No outliers were detected. Transforming the data by squaring the parameters normalized the data (K–S: $p = 0.20$; NPP: approximately linear) and corrected for heteroscedasticity (L: $p = 0.119$). The results of the ANOVA performed on the transformed data ($p < 0.001$) indicated that at least two of the parameter means differed between model types. Post hoc comparisons of the squared means showed that each model type sufficiently differed from every other model type with the exception of GRD and SGD (T–K: $p = 0.074$).

Transformation of the data (b^3) was once again required to correct for heteroscadasticity (L: $p = 0.117$) among the dense models. Normality was preserved in the transformed data (NPP: approximately linear; K–S: $p = 0.20$). The ANOVA results were significant ($p < 0.001$), indicating at least two parameter means were discernible. Fig. 4 shows the post hoc comparisons indicating that only GRD and HSM were not sufficiently distinguishable among the denser models (T–K: $p = 0.998$).

3.2. Mono-fractal dimension

Fig. 5 displays log–log graphs of the linear fits on the mono-fractal plots of box number versus box size. R^2 values are shown in Table 1. Steeper slopes indicate higher mono-fractal dimension, D_f. Values of D_f approaching the integer dimension of 3.0 correspond to volumetric structures with greater space-filling capability and more connectivity than those with D_f closer to 2.0. Hence, fractal dimensions of the dense models were higher than those of sparse models. As was the case with lacunarity, slopes of both HLG lines were clearly lower and, thus, have D_f values closer to 2.0 than to 3.0. Distinctions between the other models were not obvious from the graphs and require reliance on formal tests to reveal whether they have distinct D_f measures.

A scatter plot of the D_f values is displayed in Fig. 6. Heteroscedasticity was detected among the sparse models (L: $p < 0.001$), but NPP plots looked approximately linear and formal tests did not indicate significant deviation from normality (K–S: $p = 0.91$). Transforming the data as D_f^4 corrected for heteroscedasticity (L: $p = 0.127$). The ANOVA on D_f^4 showed significance ($p < 0.001$). The fractal dimensions for the RND and GRD models were not shown

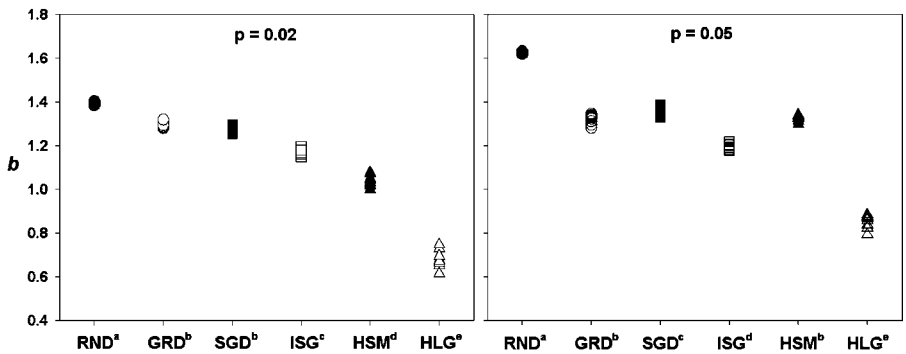

Fig. 4. Distribution of b parameters from best-fit exponential decay relationship to lacunarity results. Superscripts indicate significant differences among volumetric neutral models for a given occupancy probability.

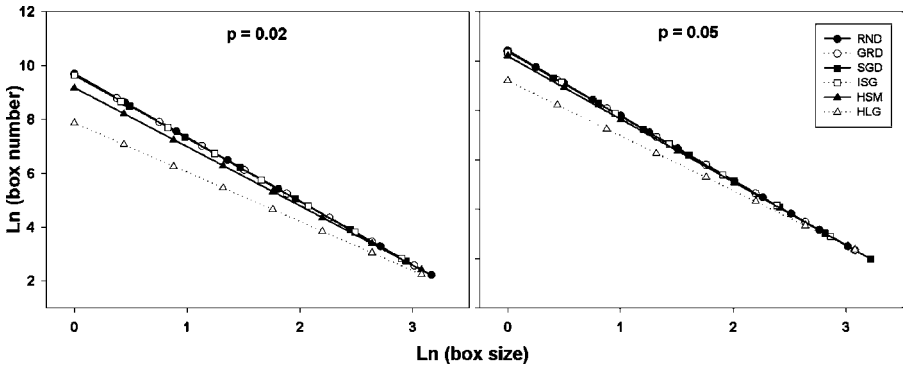

Fig. 5. Linear fits to average mono-fractal plots.

to be distinct (T–K: $p = 0.799$). A similar result was found for the SGD and ISG models ($p = 1.00$). Tests for homogeneity showed that the variances were not constant across the dense models (L: $p = 0.009$), though normality assumptions were not violated (NPP: approximately linear; K–S: $p = 0.084$). Transformations failed to correct for heteroscedasticity, so nonparametric equivalents to the ANOVA were used. Both Kruskal–Wallis and Mood Median analysis showed a difference in at least two medians ($p < 0.001$ for both procedures). At $\alpha = 0.05$, multiple Mann–Whitney post hoc comparisons did not show a significant distinction among the GRD, SGD and ISG models.

3.3. Multifractal spectra

Quadratic fits of the average multifractal spectra, $f(\alpha)$ versus α, are displayed in Fig. 7. R^2 values are shown in Table 1. Spectra of multifractal structures typically resemble a parabolic curve, as was the case with spectra calculated from the volumetric models. The graphs show how $f(\alpha)$ varies over a range of diverging exponents, α. The maxima of the concave parabolas are equivalent to the mono-fractal dimensions of the volumetric patterns but differ from the parameters calculated from the earlier box-counting method because box sizes differed from those used in calculating the multifractal indices. If any of the patterns resembled an exact mono-fractal (perfect self-similarity), the spectrum would collapse into a single point, D_f (Solé and Manrubia, 1995; Drake and Weishampel, 2000). Because all measures of $f(\alpha)$ have a unique scaling exponent, α, the volumetric patterns can more accurately be characterized as multifractals, i.e., fine-scale patterns, each possessing their own fractal dimension, embedded within coarse-scale patterns.

As with plots resulting from both lacunarity and mono-fractal analyses, the HLG parabola was clearly

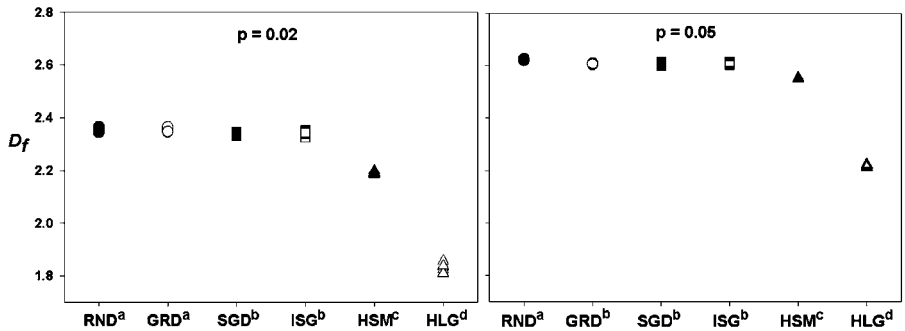

Fig. 6. Distribution of D_f parameters from best-fit linear relationship to box-counting fractal results. Superscripts indicate significant differences among volumetric neutral models for a given occupancy probability.

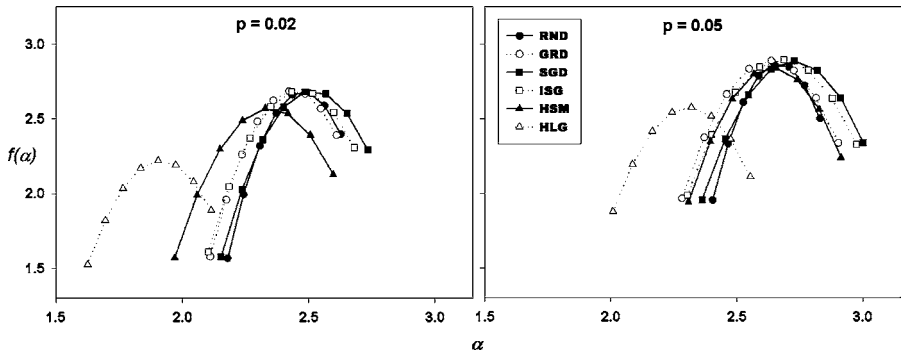

Fig. 7. Quadratic fits to average multifractal spectra.

set apart from the others for both densities with respect to apex location on both the $f(\alpha)$ and α axes. Though the location of the HSM parabola differed markedly from the other sparse models, it overlapped with RND and all three gradient parabolas derived from the dense models. The shapes were consistent within each density and the widths of the parabola spans appeared to be similar for all models. By inspection, only small variations in the apex location on the α axis can be detected of the RND and the three gradient models.

A distribution plot of the c_1 parameters, which define the apex location on the α axis and, in part, the $f(\alpha)$ axis, is shown in Fig. 8. Tests indicated no violations of normality or homogeneity of variance across sparse model types, and the ANOVA was significant ($p < 0.001$). Mean comparisons showed SGD versus ISG (T–K: $p = 0.073$) and HSM versus HLG (T–K: $p = 0.432$) as not sufficiently distinguishable by the c_1 parameters. As with the sparse models, the ANOVA of the c_1 parameters of the dense models was significant ($p < 0.001$) with tests of assumptions showing no deviations from normality or homogeneity. Pairwise comparisons showed that the means of the GRD and SGD models were not sufficiently distinct (T–K: $p = 0.823$) with similar results found between the ISG and HLG models (T–K: $p = 0.338$).

The second multifractal parameter, c_2, defines the width of the parabola. Similar to the findings for the c_1 parameters, the results of the ANOVAs performed on the c_2 parameters of the 2% and 5% models (see Fig. 9) were significant ($p < 0.001$) and no assumptions were violated. Pair-wise comparisons showed no significant difference among the 2% parameter means of the SGD, ISG, and HLG models (SGD versus ISG: $p = 0.751$; SGD versus HLG: $p = 1.00$; ISG versus HLG: $p = 0.889$). All 5% models were discernible except for the GRD and HLG models (T–K: $p = 0.431$).

The analysis of the last parameter, y_0, relating to the location on the $f(\alpha)$ axis, (Fig. 10), revealed a significant difference among the response means ($p < 0.001$)

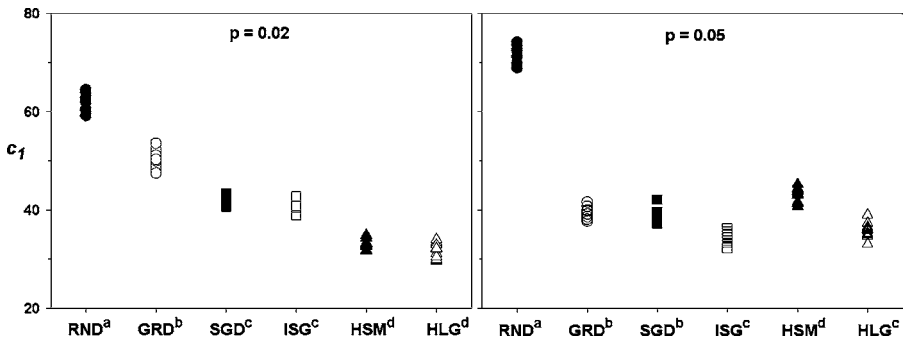

Fig. 8. Distribution of c_1 parameters from best-fit quadratic relationship to multifractal spectra. Superscripts indicate significant differences among volumetric neutral models for a given occupancy probability.

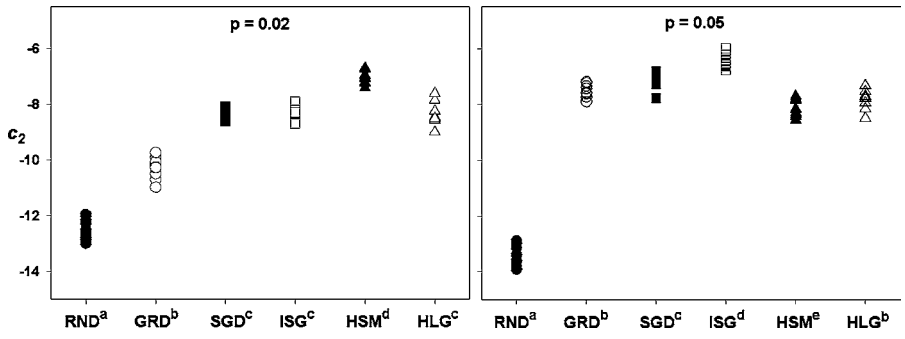

Fig. 9. Distribution of c_2 parameters from best-fit quadratic relationship to multifractal spectra. Superscripts indicate significant differences among volumetric neutral models for a given occupancy probability.

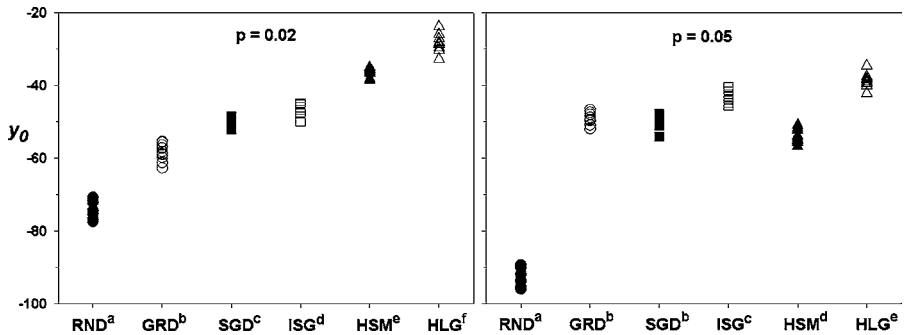

Fig. 10. Distribution of y_0 parameters from best-fit quadratic relationship to multifractal spectra. Superscripts indicate significant differences among volumetric neutral models for a given occupancy probability.

and no assumption violations for both sets of models. The y_0 parameter differed among all the sparse models. Among the dense models, only the GRD and SGD models were indistinguishable from each other ($p = 0.960$).

4. Discussion

The fits of the lacunarity results and the multifractal spectra to the exponential decay and parabolic models were very good for most models at both the low and high densities (Table 1). The exception was for the low density HLG model for lacunarity. These fits on average were better than the fits of the mono-fractal patterns to the linear model. Among the six volumetric neutral model types, the RND and HLM models were generally discernible from all other types regardless of density or the technique used. These models represent the most widely distributed, lowest density and the most concentrated, highest density models, respectively. At least one of the three gradient structures, GRD, SGD, and ISG, was not distinct from one or both of the others by four of the five parameters within both 2% (sparse) and 5% (dense) occupied models.

The density of the model did not seem to be a significant factor in each technique's capability of discerning pattern as results were similar between sparse and dense models. Within both density groups, the lacunarity measure was able to discern five models; simple fractal, four models. Parameters c_1 and c_2, which determine the location of the parabola apex on the $\alpha(q)$ axis as well as its width, were different among the four sparse models. Their sensitivity varied slightly with the dense models; c_1 discerned four models while c_2 was able to distinguish five. Only the multifractal parameter, y_0, relating to the parabola's intercept on the $f(\alpha)$ axis, was successful in distinguishing between all three sparse gradient models as well as the random and hierarchical models. It was also among the most sensitive

measures of the dense models, discriminating among five of the models. This result was somewhat unexpected because the apex of the parabola, $q = 0$, corresponds to the mono-fractal dimension. It is suspected that the wider range of box sizes used in the multifractal algorithm yielded a more accurate, and more sensitive, fractal dimension. Also, the R^2 values of the quadratic fits of the multifractal spectra were higher than those for the mono-fractal linear fits, so results may have been more distorted as some box sizes did not fully represent the structure.

Among these techniques, the three parameters characterizing the multifractal spectra clearly were more sensitive to the pattern differences among the generated structures. However, lacunarity analysis was also useful as the lacunarity plots showed that volumetric patterns deviated from self-similarity, indicating multifractal structure, reinforcing similar information provided by the multifractal spectra. The single fractal dimension, the weakest index of this study, is of limited use in distinguishing between volumetric multifractal objects and will fall short of characterizing volumetric spatial patterns. A further limitation of the mono-fractal dimension is that patterns with the same fractal dimension may have very different appearances as shown, for example, by the results for RND and GRD models. Because box-counting for the fractal dimension gives equal weight to boxes with unequal mass measure, the simple fractal dimension ignores potentially valuable information regarding underlying pattern generating processes.

This comparative neutral model approach established a statistical benchmark for the use of lacunarity, simple fractal dimension, and multifractal spectra for volumetric pattern analysis. However, further analyses are necessary to better mimic the much more subtle differences found in natural structures, e.g., canopy or coral reef architecture. For example, numerous variants using hierarchical clumping should be investigated as well as fractal (midpoint displacement) structural models or Lindenmayer systems (Sievanen et al., 2000) that depict realistic biological architectures. For forest canopies, three-dimensional, spatially explicit models could be used (Chave, 1999; Dubé et al., in press). Models with higher overall probabilities of occupied sites should be used to determine how density affects the sensitivity of the techniques. Techniques that calculate and compare autocorrelation among occupied voxels oriented to each other in specific directions (Gustafson, 1998) should be assessed for their sensitivity in detecting anisotropy, or directional orientation of pattern, in volumetric structures. Using the techniques from this study, anisotropy could also be studied by rotating the volumes and reanalyzing the structures from different orientations. Point pattern analysis techniques, such as nearest neighbor or trend surface analyses, and other methods used for quantifying spatial structure should also be adapted for three-dimensional analysis and similarly assessed for their capability in discriminating volumetric spatial patterns. Also, techniques used across disciplines to quantify random heterogeneous materials should be included (Torquato, 2002).

In summary, volumetric imaging and data mapping provides new opportunities to assess the relationship of pattern and process on ecological systems that are best described as between two and three dimensions. The neutral landscape model can continue to be a useful basis for comparison to volumetric renderings of morphological or structural data in ecological systems by generating cubic versions of the familiar planar maps. Though this study showed the multifractal approach to be best able to distinguish among the model examples, more extensive experimentation is needed to assess the behavior of additional pattern analysis techniques on a larger variety of three-dimensional data structures.

Acknowledgements

We appreciate the comments of Don Jones, David Nickerson, and two anonymous reviewers and the contributions of Susan Rawson, Elliot Vittes, and Haven Sweet. This research is based upon work supported by the U.S. National Science Foundation under Grant No. NSF #9984574. Any opinions, findings, and conclusions or recommendations expressed in this publication are those of the authors and do not necessarily reflect the views of the National Science Foundation.

References

Allan, C., Cloitre, M., 1991. Characterizing the lacunarity of random and deterministic fractal sets. Phys. Rev. A 44, 3552–3558.

Appleby, S., 1996. Multifractal characterization of the distribution pattern of the human population. Geogr. Anal. 28, 147–160.

Aykac, M., Uribe, J., Baghaei, H., Li, H.D., Wang, Y., Liu, Y.Q., Xing, T., Wong, W.H., 2002. Septa design study for volumetric imaging in positron emission tomography. IEEE Trans. Nucl. Sci. 49, 2097–2102.

Basillais, E., 1998. Functional role of the fractal morphology of corals: a full model of the nutrient turbulent diffusion fluxes to a coral reef. C. R. Acad. Sci. Paris Life Sci. 321, 295–298.

Bérubé, D., Jébrak, M., 1999. High precision boundary fractal analysis for shape characterization. Comput. Geosci. 25, 1059–1071.

Capowiez, Y., Renault, P., Belzunces, L., 2001. Three-dimensional trajectories of Co-60-labelled earthworms in artificial cores of soil. Eur. J. Soil. Sci. 52, 365–375.

Casas, J., Aluja, M., 1997. The geometry of search movements of insects in plant canopies. Behav. Ecol. 8, 37–45.

Caswell, H., 1976. Community structure: a neutral model analysis. Ecol. Monogr. 46, 327–354.

Chave, J., 1999. Study of structural, successional and spatial patterns in tropical rain forests using TROLL, a spatially explicit forest model. Ecol. Model. 124, 233–254.

Cheng, Q., 1997a. Discrete multifractals. Math. Geol. 29, 245–266.

Cheng, Q., 1997b. Multifractal modeling and lacunarity analysis. Math. Geol. 29, 919–932.

Cheng, Q., Agterberg, F.B., 1995. Multifractal modeling and spatial point processes. Math. Geol. 27, 831–845.

Dale, M.R.T., 2000. Lacunarity analysis of spatial pattern: a comparison. Landsc. Ecol. 15, 467–478.

Dechesne, A., Pallud, C., Debouzie, D., Flandrois, J.P., Vogel, T.M., Gaudet, J.P., Grundmann, G.L., 2003. A novel method for characterizing the microscale 3D spatial distribution of bacteria in soil. Soil Biol. Biochem. 35, 1537–1546.

Dougherty, G., Henebry, G.M., 2002. Lacunarity analysis of spatial pattern in CT images of vertebral trabecular bone for assessing osteoporosis. Med. Eng. Phys. 24, 129–138.

Downey, D.B., Fenster, A., Williams, J.C., 2000. Clinical utility of three-dimensional US. Radiographics 20, 559–571.

Drake, J.B., 1998. Characterizing and modeling spatial pattern of a longleaf pine savanna. Masters thesis, University of Central Florida, Orlando, 122 pp.

Drake, J.B., Weishampel, J.F., 2000. Multifractal analysis of canopy height measures in a longleaf pine savanna. For. Ecol. Manage. 128, 121–127.

Drake, J.B., Weishampel, J.F., 2001. Simulating vertical and horizontal multifractal patterns of a longleaf pine savanna. Ecol. Model. 145, 129–142.

Dubé, P., Ménard, A., Bouchard, A., Marceau, D.J., 2005. Simulating the impact of small-scale extrinsic disturbances over forest species volumetric light environment. Ecol. Model. 145, 113–129.

Falconer, K.J., 1990. Fractal Geometry: Mathematical Foundations and Applications. Wiley, New York, 288 pp.

Fitter, A.H., Strickland, T.R., 1992. Fractal characterization of root system architecture. Funct. Ecol. 6, 632–635.

Gallager, S.M., Davis, C.S., Epstein, A.W., Solow, A., Beardsley, R.C., 1996. High-resolution observations of plankton spatial distributions correlated with hydrography in the Great South Channel, Georges Bank. Deep-Sea Res. Part II-Top. Stud. Oceanogr. 43, 1627–1663.

Gardner, R.H., Milne, B.T., Turner, M.G., O'Neill, R.V., 1987. Neutral models for the analysis of broad-scale landscape pattern. Landsc. Ecol. 1, 19–28.

Gardner, R.H., O'Neill, R.V., 1991. Pattern, process and predictability: the use of neutral models for landscape analysis. In: Turner, M.G., Gardner, R.H. (Eds.), Quantitative Methods in Landscape Ecology. Springer-Verlag, New York, pp. 289–307.

Gardner, R.H., O'Neill, R.V., Turner, M.G., 1993. Ecological implications of landscape fragmentation. In: Pickett, S.T.A., McDonnell, M.J. (Eds.), Humans as Components of Ecosystems: Subtle Human Effects and the Ecology of Populated Areas. Springer-Verlag, New York, pp. 208–226.

Gefen, Y., Meir, Y., Mandelbrot, B.B., Aharony, A., 1983. Geometric implementation of hypercubic lattices with noninteger dimensionality by use of low lacunarity fractal lattices. Phys. Rev. Lett. 50, 145–148.

Gillespie, T.W., Brock, L., Wright, C.W., 2004. Prospects for quantifying structure, floristic composition and species richness of tropical forests. Int. J. Remote Sens. 25, 707–715.

Gotelli, N.J., Graves, G.R., 1996. Null Models in Ecology. Smithsonian Inst. Press, Washington, DC, 368 pp.

Green, D., 1995. Fractals and Scale. Available at: http://server.srcpc.unsw.edu.au/complex/tutorials/tutorial3.html.

Gustafson, E.J., 1998. Quantifying landscape spatial pattern: what is the state of the art? Ecosystems 1, 143–156.

Hallé, F., Oldeman, R.A.A., Tomlinson, P.B., 1978. Tropical Trees and Forests: An Architectural Analysis. Springer-Verlag, New York, 441 pp.

Hargrove, W.W., Hoffman, F.M., Schwartz, P.M., 2002. A fractal landscape realizer for generating synthetic maps. Conserv. Ecol. 6 (2) [online]. URL: http://www.consecol.org/vol6/iss1/art2.

Hewitt, R.P., Demer, D.A., 2000. The use of acoustic sampling to estimate the dispersion and abundance of euphausiids, with an emphasis on Antarctic krill, *Euphausia superba*. Fish. Res. 47, 215–229.

Keitt, T.H., Johnson, A.R., 1995. Spatial heterogeneity and anomalous kinetics: Emergent patterns in diffusion-limited predatory-prey interaction. J. Theor. Biol. 172, 127–139.

Kostylev, V., Erlandsson, J., 2001. A fractal approach for detecting spatial hierarchy and structure on mussel beds. Mar. Biol. 139, 497–506.

Lavorel, S., Gardner, R.H., O'Neill, R.V., 1993. Analysis of patterns in hierarchically structured landscapes. Oikos 67, 521–528.

Lefsky, M.A., Cohen, W.B., Parker, G.G., Harding, D.J., 2002. Lidar remote sensing for ecosystem studies. BioScience 52, 19–30.

Li, H., Reynolds, J.F., 1994. A simulation experiment to quantify spatial heterogeneity in categorical maps. Ecology 75, 2446–2455.

Mach, J., Mas, F., 1995. Two representations in multifractal analysis. J. Phys. A-Math. Gen. 28, 5607–5622.

Mach, J., Mas, F., 1997. MFRAC v2.0 Software for Fractal and Multifractal Indices Calculation. Available at: http://www.qf.ub.es/area5/jordi/mfrac.html.

Mandelbrot, B.B., 1983. The Fractal Geometry of Nature. Freeman, New York, 468 pp.

Milne, B.T., 1992. Spatial aggregation and neutral models in fractal landscapes. Am. Nat. 139, 32–57.

Milne, B.T., Johnson, A.R., Keitt, T.H., Hatfield, C.A., David, J., Hraber, P.T., 1996. Detection of critical densities associated with pinon-juniper woodland ecotones. Ecology 77, 805–821.

Mladenoff, D.J., White, M.A., Pastor, J., Crow, T.R., 1993. Comparing spatial pattern in unaltered old-growth and disturbed forest landscapes. Ecol. Appl. 3, 294–306.

Moffett, M.W., 2001. The nature and limits of canopy biology. Selbyana 22, 155–179.

Moloney, K.A., Levin, S.A., 1996. The effects of disturbance architecture on landscape-level population dynamics. Ecology 77, 375–394.

Nadkarni, N.M., Parker, G.G., Ford, E.D., Cushing, J.B., Stallman, C., 1996. The international canopy network: a pathway for interdisciplinary exchange of scientific information on forest canopies. Northwest Sci. 70, 104–108.

O'Neill, R.V., Gardner, R.H., Turner, M.G., 1992. A hierarchical neutral model for landscape analysis. Landsc. Ecol. 7, 55–61.

O'Neill, R.V., Milne, B.T., Turner, M.G., Gardner, R.H., 1988. Resource utilization scales and landscape pattern. Landsc. Ecol. 2, 3–69.

Palmer, M.W., 1992. The coexistence of species in fractal landscapes. Am. Nat. 139, 375–397.

Panahi, A., Cheng, Q., 2004. Multifractality as a measure of spatial distribution of geochemical patterns. Math. Geol. 36, 827–846.

Parker, G.G., Harding, D.J., Berger, M.L., 2004. A portable LIDAR system for rapid determination of forest canopy structure. J. Appl. Ecol. 41, 755–767.

Parrish, J.K., Hamner, W.M., 1997. Animal Groups in Three Dimensions. Cambridge University, Cambridge, 378 pp.

Pearson, S.M., Turner, M.G., Gardner, R.H., O'Neill, R.V., 1996. An organism based perspective of habitat fragmentation. In: Szaro, R.C., Johnston, D.W. (Eds.), Biodiversity in Managed Landscapes: Theory and Practice. Oxford University Press, Oxford, pp. 77–95.

Plotnick, R.E., Gardner, R.H., Hargrove, W.W., Prestegaard, K., Perlmutter, M., 1996. Lacunarity analysis: a general technique for the analysis of spatial patterns. Phys. Rev. E 53, 5461–5468.

Plotnick, R.E., Gardner, R.H., O'Neill, R.V., 1993. Lacunarity indices as measures of landscape texture. Landsc. Ecol. 8, 201–211.

PyrakNolte, L.J., Montemagno, C.D., Nolte, D.D., 1997. Volumetric imaging of aperture distributions in connected fracture networks. Geophys. Res. Lett. 24, 2343–2346.

Rappoldt, C., Crawford, J.W., 1999. The distribution of anoxic volume in a fractal model of soil. Geoderma 88, 329–347.

Scheuring, I., Riedi, R.H., 1994. Application of multifractals to the analysis of vegetation pattern. J. Veg. Sci. 5, 489–496.

Sievanen, R., Nikinmaa, E., Nygren, P., Ozier-Lafontaine, H., Perttunen, J., Hakula, H., 2000. Components of functional-structural tree models. Ann. For. Sci. 57, 399–412.

Sisodiya, S., Free, S., Fish, D., Shorvon, S., 1996. MRI-based surface area estimates in the normal adult brain. Evidence for structural for structural organization. J. Anat. 188, 425–438.

Skirvin, D.J., 2004. Virtual plant models of predatory mite movement in complex plant canopies. Ecol. Model. 171, 301–313.

Solé, R.V., Manrubia, S.C., 1995. Are rainforests self-organized in a critical state? J. Theor. Biol. 173, 31–40.

Spies, T.A., 1998. Forest structure: a key to the ecosystem. Northwest Sci. 72, 34–39.

SPSS, 1997. SigmaPlot: Transforms and Regressions. SPSS Inc., Chicago.

Stanley, H.E., 1991. Fractals and multifractals: the interplay of physics and geometry. In: Bunde, A., Havlin, S. (Eds.), Fractals and Disordered Systems. Springer-Verlag, Berlin, pp. 1–49.

Stauffer, D., 1985. Introduction to Percolation Theory. Taylor & Francis, London and Philadelphia, 181 pp.

Stetten, G., Tamburo, R., 2001. Real-time three-dimensional ultrasound methods for shape analysis and visualization. Methods 25, 221–230.

Sugihara, G., May, R.M., 1990. Applications of fractals in ecology. Trends Ecol. E vol. 5, 79–87.

Taylor, W.D., 1979. Sampling data on the bactivorous ciliates of a small pond compared to neutral models of community structure. Ecology 60, 876–883.

Thomas, W.R., Foin, T.C., 1982. Neutral hypotheses and patterns of species diversity: fact or artifact? Paleobiology 8, 45–55.

Torquato, S., 2002. Random Heterogeneous Materials: Microstructure and Macroscopic Properties. Springer, New York, 701 pp.

Turner, M.G., Gardner, R.H., Dale, V.H., O'Neill, R.V., 1989. Predicting the spread of disturbance across heterogeneous landscapes. Oikos 55, 121–129.

Turner, M.G., Gardner, R.H., O'Neill, R.V., 2001. Landscape Ecology in Theory and Practice: Pattern and Process. Springer-Verlag, New York, 401 pp.

Turner, W., Spector, S., Gardiner, N., Fladeland, M., Sterling, E., Steininger, M., 2003. Remote sensing for biodiversity science and conservation. Trends Ecol. E vol. 18, 306–314.

Weishampel, J.F., Sloan, J.H., Boutet Jr., J.C., Godin, J.R., 1998. Mesoscale changes in textural pattern of 'intact' Peruvian rainforests (1970s–1980s). Int. J. Remote Sens. 19, 1007–1014.

Weishampel, J.F., Blair, J.B., Knox, R.G., Dubayah, R., Clark, D.B., 2000. Volumetric lidar return patterns from an old-growth tropical rainforest canopy. Int. J. Remote Sens. 21, 409–415.

Weishampel, J.F., Godin, J.R., Henebry, G.M., 2001. Pantropical dynamics of 'intact' rain forest canopy texture. Global Ecol. Biogeogr. 10, 389–398.

Wiens, J.A., Crist, T.O., With, K.A., Milne, B.T., 1995. Fractal patterns of insect movement in microlandscape mosaics. Ecology 76, 663–666.

Wiens, J.A., Schooley, R.L., Weeks Jr., R.D., 1997. Patchy landscapes and animal movements: do beetles percolate? Oikos 78, 257–264.

With, K.A., Crist, T.O., 1995. Critical thresholds in species' responses to landscape structure. Ecology 76, 2446–2459.

With, K.A., King, A.W., 1997. The use and misuse of neutral landscape models in ecology. Oikos 79, 219–229.

With, K.A., Gardner, R.H., Turner, M.G., 1997. Landscape connectivity and population distributions in heterogeneous environments. Oikos 78, 151–169.

Zeide, B., 1991. Fractal geometry in forestry applications. For. Ecol. Manage. 46, 179–188.